SERBIAN JOURNAL OF ELECTRICAL ENGINEERING
Vol. 23, No. 3, October 2026, 401-436
UDC: 004.932.4:004.032.26 **DOI: https://doi.org/10.2298/SJEE2603401N**
Original scientific paper

Illumination-Adaptive Edge Enhancement Using a Hybrid DSP–DL U-Net

Milan Nikolić[1]

Abstract: This paper presents a hybrid DSP–DL system for edge enhancement in images affected by severely degraded illumination, including under- and overexposed scenes. The proposed approach integrates deterministic gradient-based operators with an illumination-aware convolutional architecture to overcome the limitations of both classical edge extraction methods and learning-based detectors under non-uniform illumination conditions. A modified U-Net architecture is used to process a five-channel input tensor composed of histogram-adjusted luminance, multiscale Sobel gradients (3×3 and 5×5), a map of global mean intensity, and a histogram-derived scene flag. Illumination adaptivity is introduced through a dynamic branching mechanism at the network input, to enable early modulation of feature extraction based on the luminance characteristics of the scene. A spatial attention module is introduced to support coherent edge reconstruction during decoding, while training of the network is guided by a dual loss formulation in which luminance consistency is balanced with gradient preservation through a learnable weighting parameter. An adaptive refinement stage further improves the edge continuity using luminance statistics and multiscale gradient cues. Quantitative evaluation is performed using five no-reference (NR) edge and structure metrics, supported by statistical validation. Within the NR evaluation framework adopted here for illumination-degraded imagery, the proposed system demonstrates improved structural consistency relative to classical Sobel operators, and shows more stable behavior based on the NR metric when compared with representative pre-trained learning-based edge detectors under the same protocol and test conditions.

Keywords: Edge enhancement, Illumination-aware processing, Hybrid DSP–DL system, U-Net architecture, Illumination-degraded images.

1 Introduction

Edge enhancement remains a fundamental operation in computer vision and image analysis, as it supports applications such as segmentation, object recognition,

[1]Singidunum University, Belgrade, Serbia, misa_aum@hotmail.com, https://orcid.org/0009-0004-0716-9586
Colour versions of the one or more of the figures in this paper are available online at https://sjee.ftn.kg.ac.rs

© *Creative Common License CC BY-NC-ND*

industrial inspection, medical imaging, autonomous systems, and structural scene interpretation. Images acquired under severely degraded illumination, including strong under-and overexposure, often exhibit weakened gradients, reduced contrast, incomplete contour transitions, and illumination-dependent structural inconsistencies. Under these conditions, edge maps become unstable, fragmented, or partially suppressed, which reduces the reliability of conventional edge enhancement techniques.

Classical digital signal processing (DSP) operators, including Sobel and Prewitt gradient operators, Laplacian-based filters, and Canny detectors, are widely used due to their computational efficiency, interpretability, and low implementation complexity [1 – 6, 12]. These operators estimate local intensity transitions using fixed convolution kernels, and can therefore provide stable low-level structural priors under many imaging conditions, although their limitations become particularly evident in poorly exposed scenes, where weakened gradients, contrast loss, and noise amplification limit edge continuity and reduce the robustness of the model to severe exposure variation.

Deep learning (DL) approaches have been developed based on adaptive, multiscale feature learning that are capable of modeling complex structural and contextual information [31]. Architectures such as U-Net [7, 8] HED (Holistically-Nested Edge Detection) [9], and RCF (Richer Convolutional Features) [10] yield strong performance on standard edge processing benchmarks through hierarchical feature extraction, multiscale fusion, and deep supervision. Many existing learning-based methods, however, are trained predominantly on datasets of well-exposed natural images, and therefore exhibit reduced stability under severely degraded illumination. Most existing architectures also do not explicitly incorporate illumination-aware feature adaptation or deterministic gradient priors derived from classical DSP operators.

In recent studies, hybrid DSP–DL formulations have been explored in which handcrafted gradient information is combined with adaptive deep feature learning [32 – 34] and illumination-aware enhancement strategies based on luminance analysis and histogram-guided processing [13, 14]. Even with these developments, however, many existing systems either treat gradient operators solely as preprocessing stages or lack explicit mechanisms for illumination-aware feature routing and adaptive refinement under extreme exposure conditions.

In response to these challenges, this paper presents a hybrid DSP–DL system for illumination-adaptive edge enhancement in under-and overexposed imagery. The proposed approach integrates deterministic multiscale Sobel priors with an illumination-aware U-Net architecture that operates on a five-channel input tensor comprising histogram-adjusted luminance information, Sobel 3×3 and 5×5 gradient maps, a global map of mean intensities, and a histogram-derived scene flag. Illumination adaptivity is introduced through a dynamic branching mechanism

that provides exposure-aware feature routing during encoding, while a spatial attention module improves edge continuity during decoding. A dual loss formulation balances luminance consistency and gradient preservation simultaneously through a learnable weighting parameter, and a subsequent adaptive refinement stage further improves edge continuity under severely degraded illumination.

The main contributions of this work can be summarized as follows:

– A hybrid DSP–DL edge enhancement framework is presented that combines deterministic multiscale Sobel priors with illumination-aware deep feature learning;
– A five-channel illumination-aware input representation is developed, in which luminance information is integrated with multiscale gradient maps, a global mean intensity map, and histogram-derived scene information;
– An illumination-aware dynamic branching mechanism is introduced for adaptive bright/dark feature routing within a modified U-Net architecture;
– A dual loss optimization strategy is designed to balance luminance fidelity and gradient preservation through a learnable weighting mechanism;
– An adaptive refinement stage is applied to improve edge continuity and suppress illumination-dependent artifacts using deterministic luminance-guided parameter selection; and
– A comprehensive evaluation framework is presented that combines no-reference (NR) edge and structure metrics, statistical validation, and qualitative analysis under illumination-degraded conditions.

The rest of the paper is organized as follows. Section 2 summarizes the DSP foundations relevant to gradient-based image processing and illumination-degraded edge enhancement. Section 3 presents a discussion of the complementary roles of deterministic DSP operators and adaptive DL components within the proposed hybrid framework. Section 4 reviews related work on classical, learning-based, and hybrid approaches to edge processing. Section 5 provides a structured overview of edge enhancement and related edge detection methods relevant to the proposed framework. Section 6 introduces the proposed illumination-aware processing pipeline, network architecture, adaptive refinement strategy, and training methodology. In Section 7, some quantitative, statistical, comparative, and qualitative evaluation results under illumination-degraded conditions are presented, and the integrated findings are discussed. Finally, Section 8 concludes the paper and outlines possible directions for future work.

2 Foundations of Digital Signal Processing

DSP forms the foundation of many image processing systems, in which an image is treated as a two-dimensional discrete signal whose local intensity

transitions contain structural information [1]. Within this framework, edge enhancement is commonly performed using gradient-based operators that estimate spatial intensity variations and emphasize contour structures corresponding to object boundaries and texture transitions.

Classical operators such as Sobel, Prewitt, and Laplacian-based filters, including the Laplacian of Gaussian (LoG), remain widely adopted due to their low computational complexity, interpretability, and stable gradient estimation [1 – 3]. Of these methods, Sobel filtering is particularly attractive because it combines gradient estimation with mild spatial smoothing, enabling efficient extraction of horizontal and vertical intensity transitions. More advanced approaches, including the Canny detector [4, 5], further improve localization and noise suppression through multistage gradient processing and non-maximum suppression. Surveys of edge processing methods [6] indicate that classical fixed-kernel operators remain sensitive to illumination degradation, contrast reduction, and noise amplification.

Under conditions of severe under- or overexposure, local intensity transitions frequently become attenuated or partially saturated, reducing the consistency of the gradient magnitude and weakening the continuity of contours. In this case, the response of fixed convolution kernels cannot be adapted to the luminance characteristics of the scene, limiting the robustness of purely deterministic filtering strategies. Nevertheless, classical gradient operators still provide valuable low-level structural priors that remain interpretable and computationally stable even under challenging illumination conditions.

Recent studies in the field of image processing have explored the integration of classical DSP operators with adaptive learning-based methods for improved robustness under challenging illumination conditions [32 – 34]. In these hybrid approaches, deterministic gradient operators provide stable gradient priors, while learning-based models perform adaptive contextual refinement. This combination improves structural consistency under illumination-degraded conditions while preserving interpretability.

3 Complementary Roles of Classical and DL Components in a Hybrid Edge Enhancement System

The proposed hybrid system combines deterministic DSP operators with adaptive DL mechanisms, with a distinct role assigned to each component within the edge enhancement process. Classical DSP operators provide deterministic gradient priors that are derived directly from local intensity transitions, while the DL component performs contextual refinement to improve the structural consistency of edge maps under severe illumination degradation.

In the proposed framework, multiscale Sobel operators generate complementary gradient responses that emphasize structural transitions at different

spatial scales and provide stable initial edge information even under exposure conditions involving reduced local contrast or partially suppressed contour visibility. The Sobel 3×3 and Sobel 5×5 gradient maps are denoted as S_3 and S_5, respectively. By preserving these Sobel gradient maps throughout the processing pipeline, interpretable structural priors are maintained during the subsequent learnable refinement stages. The DL component operates on illumination-aware feature representations that combine histogram-adjusted luminance information with Sobel 3×3 and 5×5 gradient maps, a global mean intensity map, and a histogram-derived scene flag. Through hierarchical feature extraction and dynamic feature fusion, the network refines weakened contours, suppresses illumination-dependent artifacts, and improves the structural coherence of edge transitions that may become fragmented under illumination-degraded conditions. Illumination-aware routing enables dynamic feature specialization for bright and dark scenes within a unified architecture.

Unlike purely DSP-driven pipelines, adaptive DL mechanisms provide hierarchical feature learning and contextual modeling capabilities that can address the issue of complex illumination-dependent degradation and nonlinear structural distortions [31]. DSP priors preserve explicit gradient information while supporting interpretability and structural stability under challenging illumination conditions. In the proposed scheme, deterministic gradient priors derived from classical DSP operators are therefore combined with adaptive feature representations learned through DL architectures. The complementary roles of deterministic DSP processing and adaptive DL components are summarized in **Table 1**.

Table 1

Complementary roles of DSP and DL components.

PROCESSING ASPECT	DSP COMPONENT	DL COMPONENT	ROLE IN THE HYBRID SYSTEM
Edge extraction/ gradient priors	Sobel operators (3×3 and 5×5)	Learnable feature refinement	Initial gradients followed by refinement
Contrast representation	Gradient magnitudes (S_3, S_5)	Hierarchical feature maps	Local detail with global context
Illumination robustness	Fixed-kernel filtering	Illumination-aware feature extraction	Dynamic bright/dark routing
Input information	Luminance channel Y, Sobel 3×3 and 5×5 gradient maps	Five-channel representation	Priors fused with learned features
Generalization ability	No training required	Learning from illumination-degraded data	Stability with data-driven adaptation
Structural accuracy	Pixel-level gradient estimation	Contextual edge refinement	Continuous contours with preserved detail
Data dependency	None	Requires training data	Stable priors with adaptive enhancement

4 Related Work

Edge detection has evolved from classical filter-based approaches to modern learning-driven methods. Classical techniques rely on fixed-kernel operators and deterministic decision rules, whereas more recent models extract structural information directly from data through multi-level feature learning.

Foundational operators such as Sobel, Canny, and LoG are widely used due to their low computational complexity, interpretability, and deterministic filtering principles [1 – 6]. In these methods, local intensity changes are estimated using fixed convolution kernels, which prevents adaptation to variations in illumination and exposure. Under reduced contrast or increased noise, they often produce fragmented or unstable edge maps while also failing to incorporate higher-level contextual or structural information. Prior to the widespread adoption of DL-based edge enhancement, adaptive Sobel-based selective processing methods were proposed to improve robustness under challenging imaging conditions without employing learning-based models [11].

DL-based methods overcome these limitations by learning hierarchical features in which local gradient information is integrated with high-level structural context. The U-Net architecture [7], comprehensively reviewed in [8], has demonstrated strong performance in tasks such as segmentation and edge-aware restoration. Architectures such as HED [9] and RCF [10] extend this principle through multiscale feature fusion and deep supervision, which produce structurally coherent edge representations. Progressive image restoration frameworks have also demonstrated that multi-stage refinement strategies can improve the recovery of degraded image content through intermediate supervision and cross-stage feature fusion [15].

Learning-based edge detectors generally perform well under standard imaging conditions, but their stability decreases when they are applied to under- and overexposed images. One contributing factor is that many models are trained on datasets dominated by well-exposed natural scenes, meaning that limited use is made of the simple yet reliable gradient information provided by classical operators. This limitation has motivated research on gradient-preserving objectives and Sobel-guided loss formulations, with several authors reporting improved structural consistency under illumination-degraded conditions [16].

Recent studies have also explored illumination-aware preprocessing and modeling techniques. Low-light enhancement methods are commonly applied to estimate illumination maps and global luminance characteristics [35], while histogram- and luminance-based descriptors have been used to distinguish between illumination or visibility groups, including low, ideal, and high illumination conditions as well as dark, semi-dark, and bright scenes [13, 14]. These approaches are conceptually related to the illumination-aware routing strategy adopted in the proposed system, where histogram-derived luminance

cues guide internal processing without the need for a separately trained external classifier. The development of other illumination-aware enhancement frameworks, such as edge-aware deblurring, curve-based low-light enhancement, and Retinex-inspired decomposition models [60 – 63], highlights the importance of adaptive luminance-guided processing under exposure-degraded conditions.

In many existing methods, classical gradient operators are employed only as optional or preliminary preprocessing steps, without being integrated into the core input representation of the learning model. In the proposed system, Sobel 3×3 and 5×5 gradients are incorporated directly into the input tensor, together with histogram-derived luminance information. This design means that deterministic edge priors can complement learned features, thereby supporting robust edge enhancement under varying illumination conditions while preserving interpretability within the overall processing pipeline.

Recent review studies have also highlighted the rapid development of DL methods for illumination-degraded image enhancement, including both reference-based and NR evaluation frameworks [67, 68]. These surveys emphasize the growing importance of illumination-aware processing, multiscale feature learning, and adaptive enhancement strategies in illumination-degraded imaging. The present work focuses on the issue of structurally consistent edge enhancement under severe illumination degradation through a hybrid DSP–DL framework.

5 Edge Enhancement and Related Edge Detection Approaches

Edge detection and edge enhancement methods are commonly grouped into classical gradient-based approaches and DL-based approaches [29]. In hybrid DSP–DL systems, deterministic gradient priors are combined with learned representations. Each category is characterized by distinct computational principles and design assumptions, leading to different strengths and limitations under illumination-degraded conditions. In this paper, the term ‘edge enhancement’ (or ‘edge refinement’) is used to refer to the output from the proposed system in the form of continuous-valued edge maps, while ‘edge detection’ refers to conventional detector models reported in the related literature.

Classical edge detectors estimate local intensity changes using fixed convolution kernels. Representative operators include Sobel, Prewitt, Roberts, LoG, and Canny [36, 37]. These methods are computationally efficient, interpretable, and require no training data, making them suitable for real-time inspection systems, embedded platforms, and hardware-constrained environments [38]. Their limitations are well established, and are described in [39]. Since fixed kernels cannot be adapted to varying illumination, these operators are sensitive to noise and contrast degradation, and their local processing provides limited contextual or higher-level structural information. As

a result, classical edge detectors often produce unstable or fragmented responses under conditions of severe under- or overexposure.

DL-based edge detectors learn hierarchical representations in which local gradient information is combined with high-level structural context. A theoretical link between classical convolution kernels and learned filters is reported in [40], where gradient-like structures are shown to persist within deep feature hierarchies. Representative models include HED [9] and RCF [10], and lightweight architectures such as PiDiNet [41], TEED [42], and DexiNed [43], which were designed for computational efficiency while retaining multiscale edge representations. These principles are extended in boundary detection and semantic edge detection frameworks, such as BDCN [45], CASENet [46], SEAL [47], and SED [48], by incorporating context modeling, deep supervision, and attention mechanisms for improved contour continuity and structural coherence. Related boundary-aware and edge-guided models developed for adjacent vision tasks, such as salient object detection (e.g., BASNet [44]) or image restoration and super-resolution (e.g., EdgeFormer [49]), demonstrate the importance of edge and boundary information in guiding feature learning, although these are not designed as general-purpose edge detectors and are therefore not treated as direct baselines in this paper.

Learning-based edge detectors have achieved strong performance on standard benchmarks, but they typically rely on large annotated datasets and substantial computational resources. Moreover, since end-to-end training does not explicitly preserve deterministic gradient cues, the resulting representations are often less interpretable than those produced by classical gradient-based operators and less aligned with classical edge structures. Their robustness is also reduced under severe variation in exposure [50], since most training datasets are dominated by well-exposed natural images and these models do not include explicit illumination-aware processing mechanisms. The design of the proposed hybrid DSP–DL scheme was therefore motivated by the need to retain explicit gradient priors and interpretability while introducing illumination-aware learning mechanisms for edge enhancement under illumination-degraded conditions.

Hybrid DSP–DL systems combine deterministic gradient operators with adaptive neural architectures, with the aim of balancing interpretability with data-driven learning. Rather than using classical operators solely as optional preprocessing steps, gradient information is incorporated directly into the model input or intermediate feature maps. SMA-Net [32, 33] exemplifies this strategy through the integration of Sobel-derived gradients into multi-attention convolutional blocks, resulting in improved contour stability. In other hybrid methods [51 – 53], deterministic gradient responses from classical operators are fused with CNN or ANN frameworks, yielding enhanced edge localization and increased robustness to noise. In all of these approaches, gradient-based priors

help to stabilize feature extraction and preserve a degree of structural interpretability. However, existing hybrid systems generally lack explicit mechanisms for adapting their behavior to different illumination conditions, and therefore do not fully address the issue of degradation arising from under- or overexposure.

The proposed system is based on a hybrid DSP–DL framework in which classical gradient-based priors are integrated directly into the DL pipeline. The five-channel input tensor includes Sobel 3×3 and 5×5 gradient maps, the luminance channel *Y*, a global mean intensity map, and a histogram-derived scene flag that encodes bright and dark illumination conditions. Within the network, a dynamic branching mechanism provides illumination-dependent feature routing, while spatial attention enhances edge continuity during decoding. This modular combination of deterministic priors and learned representations forms the basis for robust and interpretable edge enhancement under illumination-degraded conditions.

A comparative summary of representative methods across the main categories of edge detection approaches is provided in **Table 2.**

Table 2

Edge detection methods categorized by approach, representative models, and key characteristics.

CATEGORY	REPRESENTATIVE METHODS	KEY CHARACTERISTICS
Classical (gradient-based)	Sobel, Prewitt, Roberts, LoG, Canny [36, 37]	Fixed convolution operators, computational efficiency and interpretability, sensitivity to noise, contrast reduction, limited contextual awareness
DL-based	HED [9], RCF [10], PiDiNet [41], TEED [42], DexiNed [43], BDCN [45], CASENet [9], SEAL [47], SED [48]	Hierarchical and contextual edge representations, multiscale features, deep supervision, and attention mechanisms. Limitations include dependence on annotated datasets and large-scale computational resources, reduced interpretability
Hybrid DSP–DL	SMA-Net [32], [33] and Sobel/Prewitt fusion-based hybrid approaches [51 – 53]	Integration of gradient priors with neural models, improved edge localization and noise robustness, limited scene awareness, no explicit illumination-aware routing
Proposed system	-	Sobel 3×3 and 5×5 priors, luminance and histogram-based scene analysis, illumination-aware feature routing, attention-guided refinement, robust edge enhancement under illumination-degraded conditions

5.1 Sobel operator for gradient-based edge detection

The Sobel operator is one of the most well-established gradient-based methods for detecting edges from local intensity transitions. It was originally proposed by Sobel and Feldman [54], and relies on two convolution kernels: a horizontal gradient kernel G_x, and a vertical gradient kernel G_y. Each kernel acts as a localized mask that slides across the image to compute directional derivatives of luminance. A distinctive advantage of the Sobel design is its structure based on weighted coefficients, in which higher importance is assigned to central pixels, thereby improving robustness to noise compared with simple differential operators. The edge magnitude at each pixel is computed from the horizontal and vertical Sobel responses as follows:

$$G = \sqrt{G_x^2 + G_y^2}, \tag{1}$$

where G_x and G_y denote the Sobel responses obtained by applying the corresponding masks along the horizontal and vertical directions, respectively. The standard 3×3 Sobel kernels are:

$$\boldsymbol{G}_x = \begin{bmatrix} -1 & 0 & +1 \\ -2 & 0 & +2 \\ -1 & 0 & +1 \end{bmatrix}, \quad \boldsymbol{G}_y = \begin{bmatrix} +1 & +2 & +1 \\ 0 & 0 & 0 \\ -1 & -2 & -1 \end{bmatrix}. \tag{2}$$

To capture broader spatial gradients and improve edge continuity in low-contrast or illumination-degraded regions, an extended 5×5 Sobel kernel is also employed. This larger kernel increases the spatial support while preserving the same principle of central weighting, and typically yields smoother gradient transitions. A comparative study has shown that Sobel-based edge detection can provide stable performance under noisy or less controlled imaging conditions [12]. The 5×5 Sobel kernels used in this paper are as follows:

$$\boldsymbol{G}_x = \begin{bmatrix} -2 & -1 & 0 & +1 & +2 \\ -3 & -2 & 0 & +2 & +3 \\ -4 & -3 & 0 & +3 & +4 \\ -3 & -2 & 0 & +2 & +3 \\ -2 & -1 & 0 & +1 & +2 \end{bmatrix}, \quad \boldsymbol{G}_y = \begin{bmatrix} +2 & +3 & +4 & +3 & +2 \\ +1 & +2 & +3 & +2 & +1 \\ 0 & 0 & 0 & 0 & 0 \\ -1 & -2 & -3 & -2 & -1 \\ -2 & -3 & -4 & -3 & -2 \end{bmatrix}. \tag{3}$$

Fig. 1 illustrates the application of the edge maps generated by both the 3×3 and 5×5 Sobel operators to the standard Lena image.



(a) (b) (c)

Fig. 1 – *Generation of edge maps:* (a) *original image, edge maps obtained with* (b) 3×3 *and* (c) 5×5 *Sobel operators.*

6 Proposed Method

The proposed hybrid system is designed for illumination-robust edge enhancement in images affected by severe under- or overexposure, conditions under which conventional edge detectors and standard learning-based models often lose structural information. The overall architecture of the proposed system is shown in Fig. 2.

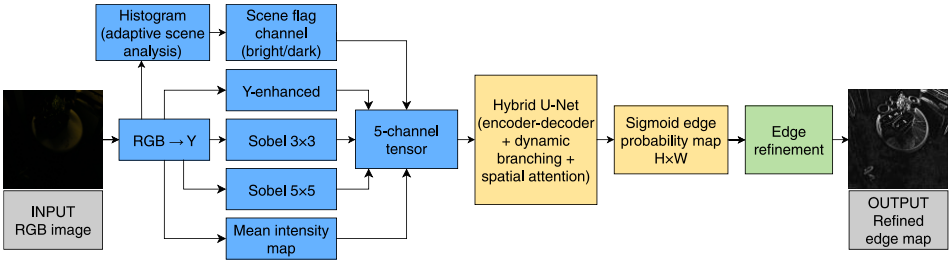


Fig. 2 – *Proposed hybrid DSP–DL system.*

Processing begins by converting the RGB input into its luminance channel Y. Two Sobel gradient maps are then computed on this channel using 3×3 and 5×5 kernels, together with a global mean intensity map. A histogram analysis of the luminance distribution produces an adjusted luminance image Y_{enhanced} and a binary scene flag indicating whether the scene corresponds to a dark (underexposed) or bright (overexposed) condition. These five components (Y_{enhanced}, the two Sobel gradients, the mean intensity map, and the scene flag) are concatenated into a single H×W×5 tensor that forms the input to a modified U-Net model.

Within the network, the initial encoder block is split into two branches that become specialized for bright and dark scenes during training. The feature maps obtained from both branches are combined through a sigmoid-based gating mechanism guided by the scene flag, enabling illumination-dependent routing of early features. A spatial attention mechanism in the decoder emphasizes coherent edge regions and suppresses unstable low-contrast responses, thereby improving edge continuity under variable illumination conditions.

Training is guided by a dual loss. For each image, the supervisory target is generated by blending the 3×3 and 5×5 Sobel responses using the fusion weights r_3 and r_5 to produce a multiscale edge map. In the loss function, a pixel-wise luminance term is combined with a gradient-preservation term computed from the magnitudes of the Sobel gradients for the predicted and target edge maps. A learnable weighting parameter controls the trade-off between these two components and is updated during training, thus allowing the global balance between luminance fidelity and gradient preservation to be learned across illumination-degraded conditions.

Following neural inference, an adaptive refinement module is applied to improve edge sharpness and stability via multiscale Sobel boosting, standard-deviation-aware sharpening, and conditional contrast adjustment derived from the luminance statistics of the predicted edge map. This stage compensates for residual edge softening and limits the appearance of halo artifacts and noise amplification under severely illumination-degraded conditions.

A summary of representative baselines and the main differences between pure Sobel filtering, generic hybrid approaches, and the proposed method is shown in **Table 3.**

6.1 System overview and processing pipeline

The proposed system consists of four adaptive processing stages, each of which operates on illumination-dependent information extracted from the input image, as follows:

– **Preprocessing and scene analysis:** The RGB input is converted into the luminance channel Y. A global histogram of this channel is then analyzed to classify the scene as bright (overexposed) or dark (underexposed).

– **Construction of the five-channel tensor:** Based on the luminance analysis, five components are prepared: the enhanced luminance Y_{enhanced}, the Sobel 3×3 and 5×5 gradient maps, the global mean intensity map, and the binary scene flag, with constant values of −1 for dark scenes and +1 for bright scenes. These five components are concatenated into an H×W×5 tensor, which serves as input to the modified U-Net model.

– **Illumination-aware neural processing**: The modified U-Net processes this tensor using an encoder–decoder structure with skip connections.

Within the network, a dynamic branching mechanism adjusts the encoder pathway according to the scene flag, while a spatial attention mechanism weights decoder features to improve edge continuity along structurally meaningful regions.

– **Edge refinement**: In the final stage, the refinement module sharpens the network output using multiscale Sobel-based amplification and luminance-aware adaptive adjustments derived from the luminance statistics of the predicted edge map. The parameters are adapted automatically in order to enhance edge contrast while limiting noise amplification and halo artifacts.

Table 3

Edge detection approaches designed for challenging illumination conditions.

ASPECT	SOBEL 3×3 AND 5×5	HYBRID APPROACHES	PROPOSED METHOD
Objective	Basic edge extraction	Edge detection via feature fusion	Edge enhancement under illumination degradation
Input data	Grayscale (Y) or RGB	RGB and intermediate features	Luminance channel *Y,* Sobel 3×3 and 5×5 gradient maps, mean intensity map, and scene flag (five-channel input tensor)
Scene adaptation	None	No explicit mechanism	Histogram-derived scene flag (bright/dark)
Preprocessing strategy	Fixed filtering	Feature embedding in CNN	Adaptive processing with dynamic branching
Architecture	Handcrafted filter	CNN with fusion modules	Extended U-Net with spatial attention mechanism and illumination-aware branches
Illumination handling	None	Limited	Explicit illumination-aware mechanisms
Edge enhancement	Not incorporated	Limited multiscale gradient fusion	Adaptive histogram-based sharpening and multiscale Sobel gradients
Evaluation approach	Basic metrics	Standard benchmarks	NR metrics, PSNR consistency measure, and scene-based qualitative analysis

6.2 Preprocessing and scene analysis

At the preprocessing stage, the RGB input is first converted into the luminance channel *Y*. This conversion process follows the ITU-R BT.601-7 formulation [55], and is implemented using MATLAB's *rgb2gray* routine, which applies equivalent coefficients as specified in [56]. For batch processing, a rounded approximation of the luminance transform is adopted:

$$Y = 0.3R + 0.59G + 0.11B, \tag{4}$$

which reduces chromatic noise and stabilizes structural consistency. A global histogram of the luminance channel Y is then computed to characterize the luminance distribution.

As illustrated in Fig. 3, this histogram serves as the basis for classification of the illumination conditions. The vertical line at mid-intensity (128) is shown for visualization purposes only. Classification is based on a comparison of the relative proportions of low- and high-luminance pixels, rather than on a fixed threshold, which allows the proposed system to perform classification dynamically.

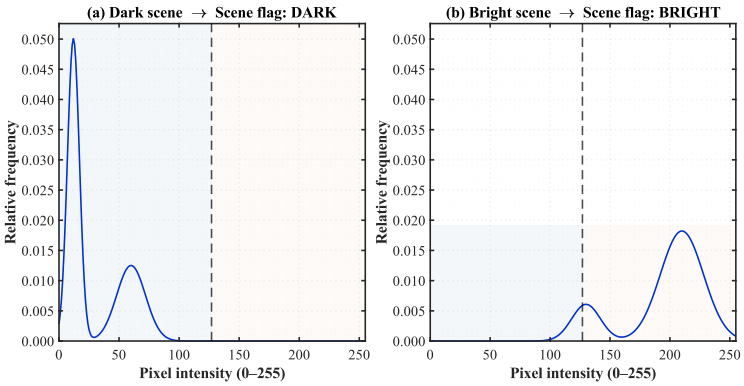


Fig. 3 – *Use of the scene flag based on the Y-channel histogram.*

Fig. 3a shows a luminance distribution that is concentrated in the lower part of the intensity range, characteristic of a dark scene; Fig. 3b shows the opposite case, where the histogram shifts toward higher intensities, representing a bright scene. If Y_i represents the luminance value of pixel i and N is the total number of pixels, these proportions are defined as:

$$P_{\text{dark}} = \frac{1}{N}\sum_{i=1}^{N} \mathrm{I}\{Y_i \in [0,126]\}, \tag{5}$$

$$P_{\text{bright}} = \frac{1}{N}\sum_{i=1}^{N} \mathrm{I}\{Y_i \in [127,255]\}, \tag{6}$$

where $\mathrm{I}\{\cdot\}$ denotes the indicator function.

A binary scene flag is assigned as follows:

– Underexposed (dark) scene: If $P_{\text{dark}} > P_{\text{bright}}$, the image is classified as underexposed, and the scene flag is set to −1.

– Overexposed (bright) scene: If $P_{\text{bright}} \geq P_{\text{dark}}$, the image is classified as overexposed, and the scene flag is set to +1.

The binary scene flag (illumination indicator) is denoted as $B \in \{-1, +1\}$, where $B = -1$ corresponds to underexposed scenes and $B = +1$ corresponds to overexposed scenes. The term 'binary' is used here to denote the two-valued categorical encoding $\{-1, +1\}$. When passed to the network, B is replicated as an constant-valued map of dimensions H×W, and is not learnable. The sigmoid function is applied only within the branching module to generate a continuous fusion weight, rather than to B itself.

Before luminance enhancement is applied, the multiscale Sobel gradient term is defined and parameterized. The maps of the 3×3 and 5×5 Sobel gradient magnitudes, denoted as S_3 and S_5, are combined using the scalar fusion coefficients r_3 and r_5. The refinement stage also involves the evaluation of a discrete set of candidate enhancement magnitudes, denoted as k, which control the strength of the luminance adjustment.

These three quantities define the search space of the adaptive optimization mechanism, and are not manually specified. Through the optimization process, this parameter space is explored automatically to identify the configuration that best enhances edges while suppressing noise.

Based on these parameters, the illumination-adaptive enhancement is defined as follows:

– For dark scenes, the Y_{enhanced} luminance is defined as:

$$Y_{\text{enhanced}} = Y - k(r_3 S_3 + r_5 S_5), \quad B = -1. \tag{7}$$

– For bright scenes, the Y_{enhanced} luminance is defined as:

$$Y_{\text{enhanced}} = Y + k(r_3 S_3 + r_5 S_5), \quad B = +1. \tag{8}$$

The parameter k controls the magnitude of luminance modulation. In the refinement stage, a related clamped boosting factor γ_b is derived from the same optimization process as that used to evaluate (r_3, r_5, k). The fusion weights r_3 and r_5 are applied to balance the contributions of the Sobel 3×3 and 5×5 gradient maps, and are computed by applying the corresponding operators to the luminance channel Y. When combined with global luminance adaptation, this multiscale gradient fusion process preserves edge information across illumination-degraded conditions. Related histogram-based enhancement strategies for multi-scene illumination conditions are discussed in [19], while methods of preserving histogram plateaus for high-contrast regions are reviewed in [20].

The resulting histogram-refined luminance Y_{enhanced} provides a stable foundation for the subsequent neural edge enhancement stage.

6.3 Five-channel tensor construction

Five distinct image channels are prepared as input to the modified U-Net model. Each channel carries a specific type of information extracted earlier in the pipeline.

The first is Y_{enhanced}, which represents the luminance image after histogram-based adjustment. Its contrast is adjusted to preserve structural visibility in both dark and bright regions. The second and third channels contain the Sobel 3×3 and 5×5 gradient maps, denoted as S_3 and S_5, respectively: the 3×3 kernel captures fine-scale edges, while the 5×5 kernel captures broader spatial intensity transitions. By using both scales, edge information can be preserved across different resolutions.

The fourth channel is the global mean intensity map, an H×W constant-valued image filled with the average luminance of the scene that provides a global reference for the overall scene brightness. The last channel encodes the scene flag, replicated as an H×W map with constant values of −1 or +1, depending on whether the histogram analysis classifies the scene as dark or bright. This flag provides global illumination context at each spatial location.

When these channels have been prepared, they are concatenated along the channel dimension to form an H×W×5 tensor, which serves as input to the modified U-Net model.

6.4 Illumination-aware neural processing

The constructed five-channel input tensor is processed by a modified U-Net model, as illustrated in Fig. 4. The encoder consists of two downsampling stages (3×3 convolution + ReLU + 2×2 max pooling), and the bottleneck contains a 3×3 convolution with 128 filters. The decoder mirrors this arrangement using transposed convolutions, with skip connections that concatenate the encoder feature maps S_1 and S_2 at matching resolutions.

In this model, an encoder–decoder backbone is extended with illumination-aware mechanisms to preserve structural details and enable adaptation to degraded illumination. During encoding, the resolution is reduced in two steps to H/4×W/4. In parallel, the number of feature maps is expanded to 128. The intermediate representations S_1 and S_2 are preserved and later reintroduced through skip connections, to ensure that fine contours are not suppressed under degraded illumination such as extreme under- or overexposure. Illumination-dependent processing is introduced at the input to the network through a dynamic branching mechanism to enable early routing of feature extraction based on the histogram-derived scene flag.

The subsequent encoder stages and the bottleneck aggregate the global illumination context conditioned by this initial routing. Two parallel convolutional paths are defined at the network input, with contributions that are conditional on

the histogram-derived scene flag $B \in \{-1, +1\}$. The branch outputs Z_{bright} and Z_{dark} are gradually fused rather than selected in a binary manner. The scene flag B is a fixed discrete indicator, and is not passed through a sigmoid function: this function is applied only to the internal branch responses to produce a continuous fusion weight w_{light}, thereby enabling soft blending of the bright and dark feature pathways. The fusion coefficient w_{light} is determined by the sigmoid-based weighting function, and the blended activation map Z is obtained as follows:

$$w_{\text{light}} = \frac{1}{1+\exp\left[-k(B-0.5)\right]}, \tag{9}$$

$$Z = w_{\text{light}} \cdot Z_{\text{bright}} + (1 - w_{\text{light}}) \cdot Z_{\text{dark}}. \tag{10}$$

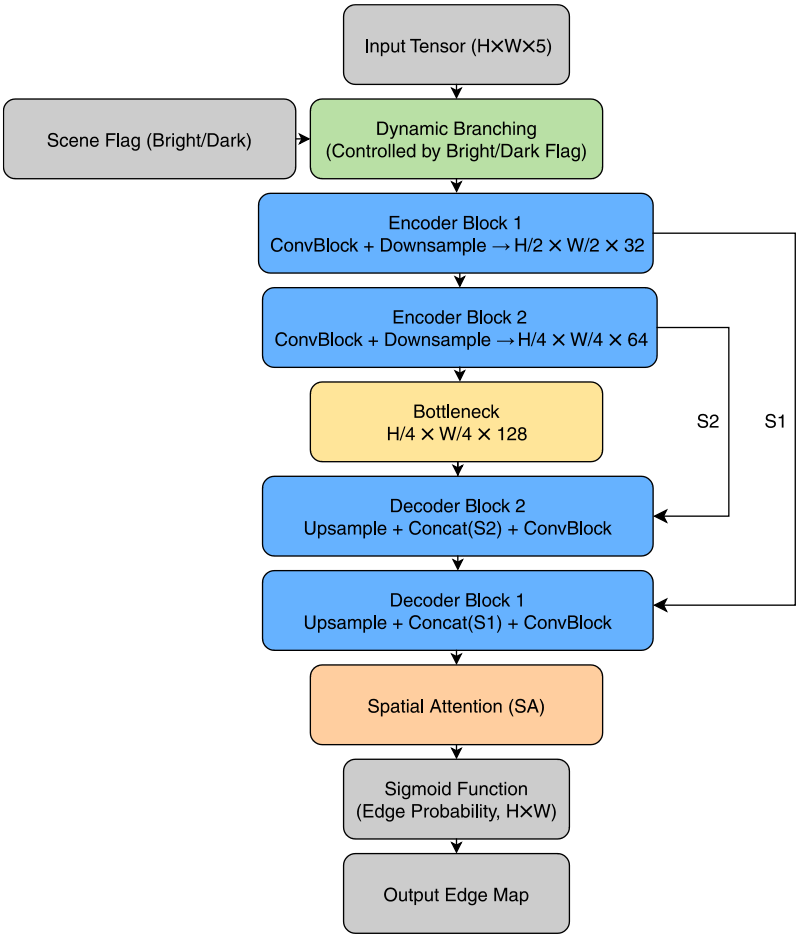


Fig. 4 – *Architecture of the proposed illumination-aware U-Net with dynamic branching and spatial attention.*

Here, the scene flag B acts as a fixed global indicator of the exposure of the scene, while the sigmoid function produces a continuous fusion weight w_{light}, enabling smooth interpolation between the bright and dark feature pathways. This mechanism creates a continuous transition between illumination domains without the need for manually defined exposure thresholds, and allows bright and dark scenes to be processed by the same backbone without discrete mode switching. Since the branch fusion process is based on continuous sigmoid weighting rather than hard binary selection, scenes near the midpoint between bright and dark exposure conditions are processed through gradual feature interpolation instead of abrupt routing transitions. Consequently, scenes with mixed illumination may activate both feature pathways simultaneously, enabling smoother adaptation to intermediate exposure characteristics. Although the proposed routing mechanism is designed to improve robustness across diverse exposure conditions, highly heterogeneous scenes with strong local illumination imbalance may remain challenging, and the model could benefit from future extensions based on spatially adaptive exposure estimation.

For further stabilization of feature localization, spatial attention is applied after the branching stage, following the principle introduced in [17]. The attention unit amplifies coherent gradient regions and, conversely, suppresses unstable low-contrast responses and residual noise, thereby improving edge continuity in the subsequent decoding stage. In the decoder, the original resolution H×W is restored, and S_1 and S_2 are injected through skip pathways so that local transitions are reconstructed together with global luminance cues accumulated in the bottleneck.

The predictions of the model are constrained by a sigmoid output layer, which provides a continuous-valued edge field in the normalized range [0, 1], thereby supporting both visual inspection and quantitative evaluation. Training is based on a dual loss formulation in which luminance fidelity and gradient preservation are optimized jointly. The loss function is:

$$L_{\text{total}} = \mathrm{s}(\lambda_{\text{raw}}) \cdot L_{\text{edge}} + \left(1 - \mathrm{s}(\lambda_{\text{raw}})\right) \cdot L_1, \tag{11}$$

where $\mathrm{s}(\cdot)$ denotes the loss-weight sigmoid transform applied to the learnable parameter λ_{raw}, as distinct from the sigmoid function used in the branching module. The effective coefficient $\mathrm{s}(\lambda_{\text{raw}})$ is constrained to the interval [0, 1], providing a bounded trade-off between the L_1 and L_{edge} terms. L_1 is used to evaluate direct pixel-wise deviation, while L_{edge} measures the difference between the Sobel 3×3 and 5×5 gradient magnitude fields of the prediction and the target.

The parameter λ_{raw} is implemented as a single, globally learnable scalar that is shared across all training samples, rather than as an image-specific weight. It is initialized from a zero-mean Gaussian distribution to avoid imposing a systematic initial preference for either loss term after the sigmoid transformation.

Although one loss component may contribute more strongly due to different numerical magnitudes, this sigmoid-bounded formulation prevents either term from being assigned an exact zero coefficient. Consequently, both loss components remain explicitly active, and the learned scalar defines a global balance between luminance fidelity and gradient preservation across the training set. Supervisory edge targets used for training are not manually annotated, and are generated automatically by blending the Sobel 3×3 and Sobel 5×5 responses into a single multiscale reference.

Designs for lightweight encoder–decoder models, including U-Net variants with reduced depth and an orientation towards efficiency, have been explored in [57, 58]. In this work, the same efficiency rationale is adopted to ensure computational feasibility for five-channel 512×512 inputs in CPU-bound environments.

To further improve the robustness under degraded illumination conditions, the dataset is expanded offline using exposure-oriented data augmentation techniques [59]. The training pipeline generates multiple variants of each image, exclusively for training and validation, based on controlled illumination scaling, gamma modulation, and noise injection. Brightening and darkening factors are used to simulate severe over- and underexposure, while gamma adjustments introduce nonlinear luminance variations. In addition, Gaussian and salt-and-pepper noise is applied to model the intensity fluctuations that are commonly observed in illumination-degraded scenes. These augmentations increase the exposure diversity in the training set and improve the generalization ability of the model across extreme illumination conditions, thereby improving the consistency and stability of the resulting edge maps. From a set of 500 original images, the offline augmentation pipeline generated 5,000 training pairs, which were randomly partitioned into training and validation subsets using an 80/20 split, yielding 4,000 training pairs and 1,000 validation pairs. An independent test set of 32 previously unseen illumination-degraded images was used for the final evaluation. Test images were evaluated in their original, unmodified form.

6.5 Edge refinement module

Although the proposed illumination-aware U-Net provides edge predictions that are robust to variations in exposure, residual edge softening and mild halo artifacts may still be present under severely degraded illumination. Classical sharpening operators, such as Laplacian and unsharp-mask-based enhancement methods [18], are generally based on fixed deterministic behavior, meaning that they provide limited adaptability under severely varying illumination. Existing enhancement strategies, including edge-aware deblurring, low-light enhancement, and Retinex-inspired models [60 – 63], often operate as single-pass procedures, and may therefore be unable to preserve edge continuity and suppress illumination-dependent noise simultaneously under extreme exposure conditions.

To mitigate these effects, the proposed system includes an adaptive edge refinement module that combines multiscale Sobel boosting with contrast-aware sharpening and illumination-guided enhancement strategies. The refinement process is designed to selectively strengthen boundary transitions while suppressing noise amplification and over-sharpening through adaptive parameter selection derived from luminance statistics and gradient responses.

Illumination-adaptive edge boosting: In the first enhancement stage, the prediction of the U-Net is reinforced using Sobel-based multiscale gradients. The strength of the enhancement is estimated dynamically from the optimal configuration (r_3, r_5, k), obtained by maximizing the luminance-driven score function defined in (20) over a discrete parameter set using global mean and standard deviation. All refinement parameters are selected automatically. The capped boosting factor γ_b is defined as

$$\gamma_b = \min(|f_{\text{final}}|, 0.4). \tag{12}$$

The enhancement factor k defined in (7) and (8) is converted into a signed boosting factor using the scene flag, as follows:

$$\text{final factor} = B \cdot k, \quad B \in \{-1, +1\}. \tag{13}$$

The magnitude of this value is then capped at 0.4 to prevent excessive amplification. The direction of enhancement is governed by the scene flag $B \in \{-1,\ +1\}$, enabling sign-aware integration of multiscale Sobel gradients as follows:

$$Y_{\text{boosted}} = Y_{\text{refined}} - \gamma_b (r_3 S_3 + r_5 S_5), \quad B = -1 \text{ (dark scene)}, \tag{14}$$

$$Y_{\text{boosted}} = Y_{\text{refined}} + \gamma_b (r_3 S_3 + r_5 S_5), \quad B = +1 \text{ (bright scene)}, \tag{15}$$

where S_3 and S_5 are the Sobel 3×3 and 5×5 gradient magnitude maps, and r_3 and r_5 are multiscale weighting coefficients selected through the score-based procedure defined in (20). This stage restores suppressed edges in underexposed regions and prevents halo exaggeration in overexposed regions while preserving the valid range:

$$0 \le Y_{\text{boosted}} \le 1. \tag{16}$$

Standard-deviation-aware sharpening: In the second refinement stage, sharpening intensity is regulated using the standard deviation σ_y of Y_{boosted}. The sharpening coefficient is defined as:

$$\alpha = \begin{cases} 0.4, & \sigma_y < 0.1, \\ 0.5, & 0.1 \le \sigma_y < 0.3, \\ \max(0.2, \min(0.7, 0.8 - 2\sigma_y)), & \sigma_y \ge 0.3. \end{cases} \tag{17}$$

Here, α is a data-driven sharpening coefficient derived from σ_y. It is not a learnable parameter and is not optimized during training, serving instead as a deterministic post-processing factor. In this design, learning-based edge prediction is explicitly separated from deterministic post-processing to improve interpretability and stability. The sharpened luminance is then:

$$Y_{\text{sharp}} = Y_{\text{boosted}} - \alpha \nabla^2 Y_{\text{boosted}}, \tag{18}$$

where σ_y represents global contrast strength, and ∇^2 denotes the Laplacian operator. This process enhances faint boundaries in low-contrast regions while avoiding overshoot in high-variance texture regions.

Multi-stage adaptive enhancement: In the final stage, edge continuity is improved and illumination-dependent noise is mitigated using conditional enhancement strategies. For extremely low-contrast scenes, a contrast-governed enhancement factor γ_c is applied, as follows:

$$\gamma_c = 1.2 + (0.06 - \sigma_y) \cdot 5, \quad \sigma_y < 0.06, \tag{19}$$

where σ_y denotes the global standard deviation of the boosted edge map, and 0.06 serves as a low-contrast activation threshold selected empirically based on a small validation subset. A value of five is introduced to regulate enhancement sensitivity, and the base value 1.2 supports controlled contrast lift without introducing halo amplification.

Additional operations include nonlinear exposure-guided transforms (tanh, sigmoid, gamma), adaptively selected based on luminance statistics, and selective Gaussian smoothing, which is applied to dark, low-variance regions to suppress noise while preserving structural boundaries.

When applied together, these adaptive procedures provide a stable balance between perceptual sharpness and smoothness under a range of illumination-degraded conditions. As summarized in **Table 4**, the refinement module mitigates the primary illumination-dependent degradation effects that remain after neural edge prediction.

Table 4

Mapping of U-Net prediction artifacts to refinement solutions.

U-NET ARTIFACT	VISUAL IMPACT	REFINEMENT SOLUTION
Suppressed edges in underexposed regions	Missing boundaries	Scene-adaptive Sobel boosting
Halo artifacts in overexposed areas	Glow around edges	Illumination-aware contrast-regulated sharpening
Noise amplification in shadows	Grainy edges, instability	Locally selective smoothing
Slight structural blurring	Soft transitions	Nonlinear contrast enhancement

Through a combination of multiscale Sobel guidance with adaptive illumination-aware refinement, the proposed module is designed to improve edge continuity and structural consistency under illumination-degraded conditions while reducing halo artifacts and illumination-dependent noise amplification.

6.5.1 Dynamic parameter selection

Unlike conventional enhancement pipelines that depend on fixed, hand-tuned values, a per-image adaptive selection strategy is applied in the refinement module. All quantities that govern this process are derived from luminance statistics and multiscale gradient cues rather than preset constants. As a result, the system responds directly to scene illumination, contrast variation, and illumination-induced degradation effects.

For each input image, the module automatically determines:

– multiscale Sobel gradient weights (r_3, r_5),

– a histogram-derived luminance scaling factor,

– the adaptive sharpening intensity,

– the sign of the illumination $B \in \{-1, +1\}$ derived from the histogram distribution, and

– normalization limits and smoothing triggers based on variance thresholds.

Parameter selection is executed using a score-based selection procedure:

$$\text{Score} = a \cdot \sigma(Y_{\text{mod}}) + b \cdot \mu(Y_{\text{mod}}). \tag{20}$$

Here, Y_{mod} represents the candidate-modified luminance, $\sigma(\cdot)$ denotes the global standard deviation, and $\mu(\cdot)$ denotes the global mean intensity. The coefficients a and b regulate the balance between structural contrast and luminance stability; these are fixed global parameters that are applied consistently across the entire evaluation pipeline, with values that are empirically selected to balance contrast enhancement and luminance preservation across both under- and overexposed conditions. Direct optimization of the NR metrics is not applied, since individual NR measures may favor excessive sharpening or noise amplification when optimized independently. Instead, the proposed score function provides a stable deterministic criterion for adaptive parameter selection based on both luminance and structural statistics. This process favors configurations that improve structural contrast while preserving luminance stability, thereby discouraging excessive amplification and contrast collapse.

A discrete set of parameter configurations (r_3, r_5, k) is evaluated, and the configuration that maximizes the score function is adopted. All refinement parameters are computed adaptively and deterministically from image statistics, with no need for manual per-image tuning or learning-based optimization. This strategy prevents over-amplification in images with strong gradients and avoids contrast suppression when structural detail is weak. Empirically selected variance

thresholds are then fixed across the evaluation pipeline to ensure stable and repeatable behavior under both underexposed and overexposed conditions.

6.6 Architectural synergy: DSP and DL integration

Classical DSP provides stable gradient priors, while the modified U-Net incorporates illumination-aware mechanisms and hierarchical feature representation. Within the proposed hybrid formulation, deterministic gradient cues are complemented by network-learned multiscale refinements, thereby supporting edge consistency under severely degraded illumination.

Sobel-based priors provide a deterministic gradient reference even when luminance distributions collapse under severe under- or overexposure. In parallel, the illumination-aware U-Net applies dynamic branching and spatial weighting to mitigate halo amplification and exposure-induced noise propagation, while preserving contour continuity across varying illumination conditions.

As a whole, the hybrid system combines deterministic DSP operators with deep feature learning mechanisms within a modular hybrid architecture. This preserves the interpretability of explicit gradient processing while enabling illumination-aware refinement of edge structures.

Table 5 summarizes the combined DSP and DL processing stages of the proposed hybrid system.

Table 5

DSP and DL processing stages in the proposed hybrid edge enhancement system.

STAGE	DSP INPUT	DL COMPONENT/ OPERATION	ROLE
Input preparation	Luminance channel, Sobel 3×3 and 5×5 gradients, mean intensity map, and scene flag	Five-channel U-Net input	Provides structural and illumination information
Illumination adaptation	Histogram-derived scene flag	Dynamic bright/dark branching	Supports exposure-aware feature routing
Edge reconstruction	Multiscale Sobel gradient information	U-Net with skip connections and spatial attention	Improves contour continuity and structural consistency
Training guidance	Sobel-blended supervisory target	Dual loss formulation	Balances luminance fidelity and gradient preservation
Final refinement	Luminance statistics and multiscale Sobel boosting	Adaptive refinement after neural prediction	Strengthens weak edges while limiting noise and halo artifacts

7 Evaluation and Statistical Validation of Results

7.1 Quantitative analysis with NR metrics and statistical validation

The proposed hybrid system was evaluated based on real illumination-degraded images containing both under- and overexposed scenes. Since reliable ground truth edge annotations were unavailable for these scenes, the peak signal-to-noise ratio (PSNR), a widely used full-reference metric of image quality [21], was computed only with respect to the multiscale Sobel-blended supervisory target used during training. It is therefore reported here solely as a consistency measure, while the comparative assessment relies on five NR edge and structure metrics. An NR framework is adopted to enable fair and meaningful assessment of under- and overexposed images, consistent with reference-free methodologies for illumination-degraded imagery [23, 30]. The NR metrics were selected because they describe complementary properties of the quality of the edge maps, rather than a single isolated visual attribute. The Tenengrad measure and the variance of Laplacian (VoL) quantify the gradient strength and focus-related sharpness, standard deviation (Std) reflects the global contrast dispersion, spatial frequency magnitude (SFM) captures the spatial activity and structural density, and edge density describes the spatial coverage of the detected edge responses. Collectively, these five metrics characterize the edge strength, contrast, structural activity, and edge map coverage under illumination-degraded conditions.

These metrics were computed for each test image and reported for the AI-refined output and the two classical Sobel baselines, as follows:

- **Tenengrad**: This is a gradient-based sharpness magnitude derived from Sobel responses, and is widely adopted as an NR indicator of edge strength and structural clarity in illumination-degraded imagery [22 – 24];
- **VoL**: This is a second-order focus indicator reflecting edge prominence [23, 25];
- **Std**: This is a global contrast dispersion descriptor frequently used for scoring NR sharpness and image quality [23];
- **SFM**: This is obtained as a frequency-domain estimate of structural density derived from gradient and spectral energy distributions [23, 28], with related frequency-based NR sharpness measures [27];
- **Edge density**: This is calculated as the proportion of edge pixels indicating structural coverage, used as an NR structural coverage indicator [26]; it is interpreted as a structural coverage indicator rather than a standalone quality metric, and is therefore evaluated jointly with other NR measures to avoid rewarding noise amplification.

All five of these indicators are typically used for NR image-quality assessment because no single NR metric can fully represent the human perception of edge

continuity. The metrics are therefore interpreted jointly and comparatively here, rather than as independent scores of absolute quality.

As shown in **Table 6**, the AI-refined edge maps have elevated mean values for Tenengrad, VoL, SFM, and edge density relative to both Sobel operators. The slight increase in Std observed for the Sobel 5×5 outputs is primarily due to amplification of fine-scale variations rather than coherent structural detail. In comparison, the AI-based refinement maintains a controlled range of variance while supporting higher gradient continuity and broader edge coverage under illumination-degraded conditions. This observation further supports the interpretation of NR metrics as complementary indicators rather than absolute quality measures.

Table 6
Mean and standard deviation ($\mu \pm \sigma$) *of NR edge and structure metrics across all test images.*

METHOD	TENENGRAD	VOL	STD	SFM	EDGE DENSITY
AI-refined	0.074 ± 0.067	0.146 ± 0.144	0.191 ± 0.110	0.00039 ± 0.00022	0.339 ± 0.196
Sobel 3×3	0.038 ± 0.048	0.057 ± 0.072	0.131 ± 0.113	0.00022 ± 0.00019	0.170 ± 0.181
Sobel 5×5	0.051 ± 0.045	0.066 ± 0.066	0.233 ± 0.138	0.00028 ± 0.00017	0.286 ± 0.213

For statistical validation of these differences, paired t-tests were conducted for each NR metric to compare the AI-refined results against both classical baselines. A significance threshold of $p < 0.05$ was adopted, in accordance with standard statistical reporting practices in engineering and image-analysis research [64, 65]. This threshold was used to assess whether observed differences were statistically significant, with the trends for each metric evaluated across all test images. In view of the paired experimental design, statistical significance was interpreted jointly with consistent effect trends observed across images and metrics, rather than in isolation for individual comparisons. *p*-values are reported as a measure of statistical compatibility, and are interpreted jointly with effect trends and ($\mu \pm \sigma$) statistics, rather than as standalone evidence of practical superiority.

Table 7 shows statistically significant differences between the AI-refined method and both Sobel operators under this evaluation protocol. Together with the mean trends in **Table 6**, these results indicate consistent behavior of the proposed system in terms of these metrics, with improved edge continuity and structural coverage relative to the classical Sobel baselines under illumination-degraded conditions.

Table 7
Paired t-test results for AI vs. classical methods (p-values).

METRIC	AI VS. SOBEL 3×3 (p)	AI VS. SOBEL 5×5 (p)	STATISTICALLY SIGNIFICANT ($p < 0.05$)
Tenengrad	3.71e–06	2.26e–04	Yes
VoL	5.23e–06	2.52e–05	Yes
Std	3.32e–08	1.29e–04	Yes
SFM	4.70e–11	1.15e–08	Yes
Edge density	1.52e–08	2.58e–03	Yes

7.2 Visual and qualitative assessment

Visual comparison was conducted to complement the quantitative analysis. Fig. summarizes the mean values of all five NR metrics together with their corresponding standard deviations. Error bars represent ±1 standard deviation and correspond directly to the reported (μ ± σ) statistics in **Table 6**. The values for the Tenengrad, VoL, SFM, and edge density metrics are higher for the AI-refined outputs than for both Sobel baselines, with a controlled range of variance across the evaluated images.

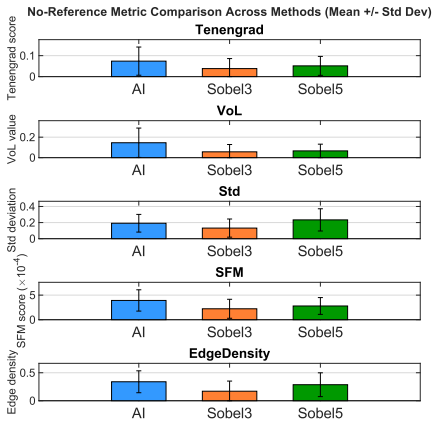
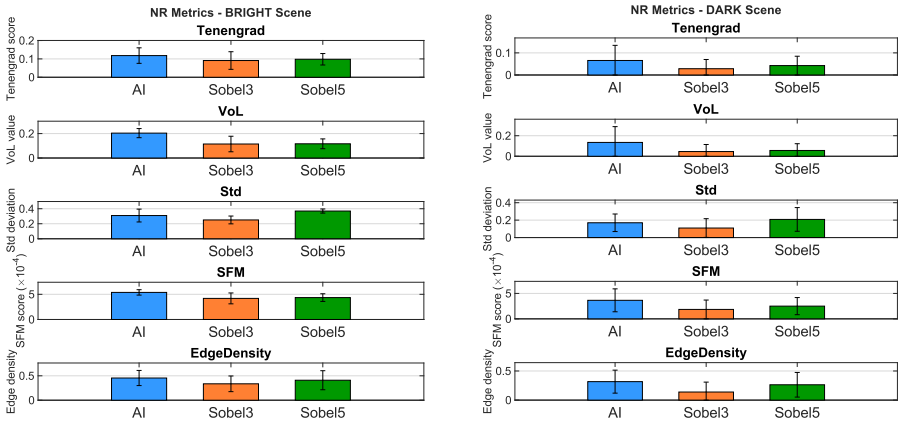


Fig. 5 – *Comparison of NR metrics (mean ± standard deviation).*

Fig. 6 shows the scene-based separation of NR metrics for images with bright and dark illumination. The results confirm that the observed performance trends persist under both illumination conditions.



(a) (b)

Fig. 6 – *Comparison of scene-based NR metrics:* (a) *bright scenes,* (b) *dark scenes.*

Fig. presents boxplot distributions for all NR metrics. It can be seen that the distributions of the AI-refined outputs support the interpretation of improved consistency and stable edge continuity across illumination-degraded conditions.

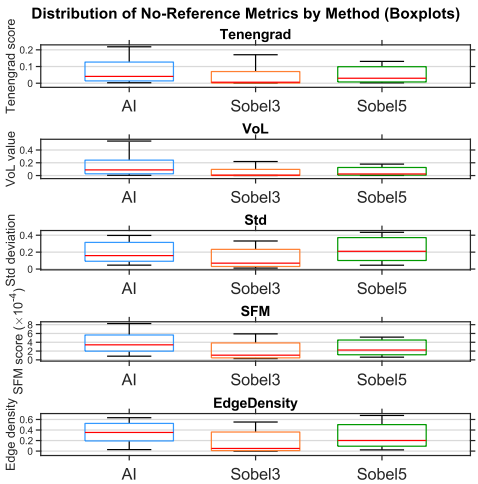


Fig. 7 – *Distributions of NR metrics (boxplots).*

Fig. 8 presents per-image heatmaps for all five NR metrics. In the majority of cases, the AI-refined edge maps show stronger gradient responses, indicating stable structural continuity.

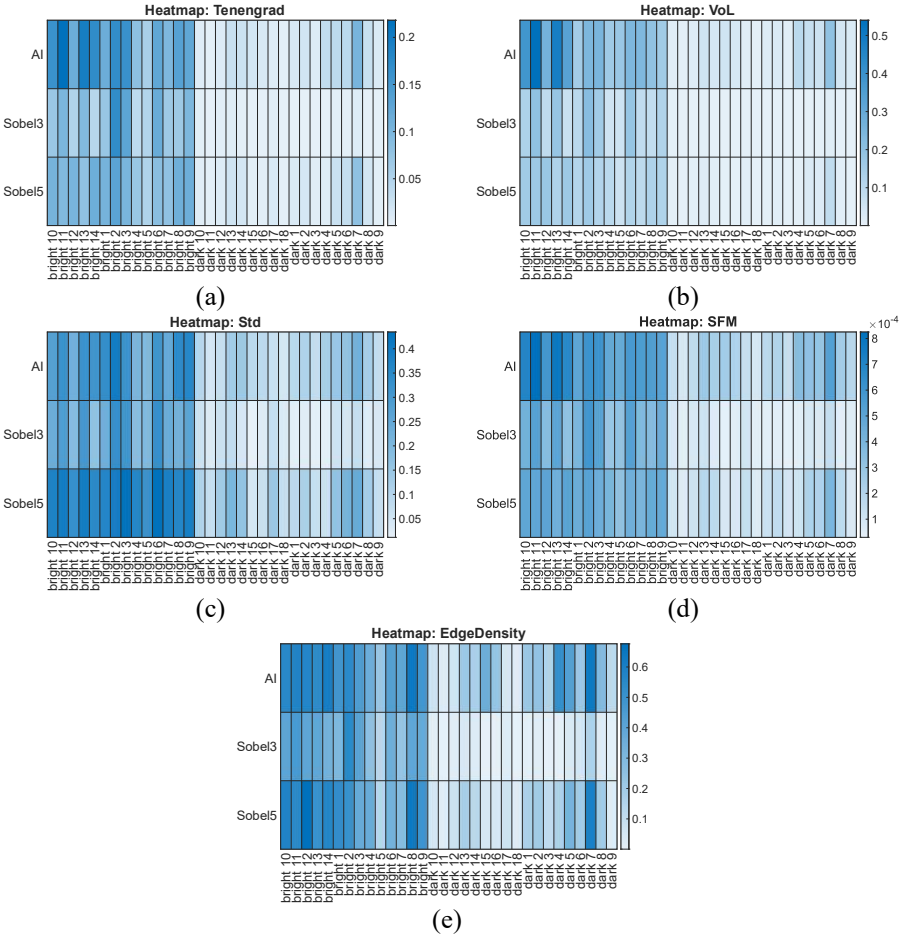


Fig. 8 – *Per-image NR metric heatmaps:* (a) *Tenengrad,* (b) *variance of Laplacian (VoL),* (c) *standard deviation (Std),* (d) *spatial frequency magnitude (SFM), and* (e) *edge density. Rows correspond to AI-refined, Sobel* 3×3*, and Sobel* 5×5 *outputs, while columns represent individual test images grouped by illumination condition.*

Taken together, the visual results are aligned with the findings of the NR quantitative analysis, and confirm stable edge formation under illumination-degraded conditions. This combined quantitative–qualitative evaluation strategy follows recommendations from recent studies of illumination-specific sharpness assessment, where NR metrics and visual inspection are interpreted jointly to evaluate the gradient continuity and edge integrity under varying exposure conditions [23, 66].

Fig. 9 presents a comparison of representative edge responses. Classical Sobel operators produce incomplete or halo-amplified contours under extreme

exposure variation, whereas the AI-refined output preserves structural boundaries with substantially reduced noise, in line with the objectives of the proposed hybrid system.



(a) (b) (c) (d)

Fig. 9 – *Qualitative comparison of edge maps:* (a) *Y-channel input image,* (b) *Sobel* 3×3*,* (c) *Sobel* 5×5*,* (d) *AI-refined output.*

7.3 Performance comparison with baseline methods

To provide a comparative context for the proposed hybrid refinement system, edge maps produced with the classical Sobel 3×3 and 5×5 operators and three publicly available pre-trained edge detection models, PiDiNet [41], DexiNed [43], and TEED [42], were evaluated under the same framework for the NR edges and structure metrics. These reference models were selected as representative

examples of contemporary learning-based edge detection methods. More specifically, PiDiNet, DexiNed, and TEED were chosen because they are lightweight, publicly available edge detectors that directly output dense edge maps, enabling fair comparison under an NR evaluation framework without additional retraining or task-specific adaptation. Each reference model was used in its publicly released pre-trained form, without modification or fine-tuning. To ensure compatibility across methods, all predicted edge maps were uniformly rescaled to an intensity range of [0, 1] before computation of the NR metrics. This normalization step affects only the input to the evaluation process, and does not change the internal behavior or inference characteristics of the reference models.

Table 8 summarizes the mean and standard deviation ($\mu \pm \sigma$) of the five NR metrics for the classical baselines, the representative learning-based detectors, and the proposed hybrid output.

Table 8
NR metrics ($\mu \pm \sigma$) for the baseline methods and proposed hybrid system across all test images.

METHOD	TENENGRAD	VOL	STD	SFM	EDGE DENSITY
Sobel 3×3	0.038 ± 0.048	0.057 ± 0.072	0.131 ± 0.113	0.00022 ± 0.00019	0.170 ± 0.181
Sobel 5×5	0.051 ± 0.045	0.066 ± 0.066	0.233 ± 0.138	0.00028 ± 0.00017	0.286 ± 0.213
PiDiNet	0.010 ± 0.009	0.014 ± 0.012	0.068 ± 0.036	0.00013 ± 0.00007	0.121 ± 0.105
DexiNed	0.007 ± 0.006	0.016 ± 0.016	0.047 ± 0.027	0.00012 ± 0.00008	0.130 ± 0.144
TEED	0.109 ± 0.132	0.313 ± 0.382	0.143 ± 0.132	0.00045 ± 0.00043	0.082 ± 0.098
AI-refined	0.074 ± 0.067	0.146 ± 0.144	0.191 ± 0.110	0.00039 ± 0.00022	0.339 ± 0.196

The results indicate that under this evaluation protocol, the proposed hybrid system yields higher mean values for the Tenengrad, VoL, SFM, and edge density than the classical Sobel operators and the PiDiNet/DexiNed baselines, while preserving moderate variance across all metrics. In this evaluation setting, the TEED results show higher mean values for several NR metrics (Tenengrad, VoL, and SFM) compared with the proposed system, accompanied by substantially larger standard deviations for these metrics, indicating increased sensitivity to illumination variation across scenes. The proposed system demonstrates stable behavior in terms of the metrics and elevated edge density values under illumination-degraded conditions, indicating that the resulting edge representations remain structurally coherent across diverse exposure scenarios while avoiding excessive noise amplification and halo artifacts.

7.4 Findings and discussion

As a whole, the results indicate that the proposed hybrid system yields improved edge continuity and structural coherence relative to classical Sobel operators, as reflected in generally higher mean NR metric values and statistically significant differences across NR metrics ($p < 0.05$) under the evaluation framework considered here. Visual analyses across both bright and dark scenes support these trends, as they demonstrate more continuous contours and reduced illumination-induced artifacts.

When evaluated under a unified NR assessment framework, contemporary learning-based detectors exhibit either weaker responses (PiDiNet, DexiNed) or increased variability (TEED), whereas the proposed hybrid system demonstrates a more balanced performance profile characterized by elevated edge density and controlled variance. These findings suggest that the integration of explicit gradient priors with illumination-aware routing and adaptive refinement provides stable edge enhancement across diverse illumination-degraded scenarios.

The comparisons with PiDiNet, DexiNed, and TEED presented above are intended to reflect the relative behavior of these models under illumination-degraded conditions within this NR evaluation framework, rather than to imply general performance rankings across domains, supervision regimes, or training settings.

The evaluation protocol adopted here does not replace full-reference assessment or formal human perceptual validation. Since reliable manually annotated ground truth edge maps are not available for the illumination-degraded test images, PSNR is used only as a consistency indicator relative to the Sobel-blended supervisory target. A limited full-reference evaluation using manually annotated edge maps or a controlled human perceptual study could further strengthen the validation of the proposed system, but such assessments fall outside the scope of the present study.

8 Conclusion

8.1 Summary of the proposed approach

This work has presented a hybrid edge enhancement system in which deterministic DSP priors are combined with illumination-aware DL to improve edge representations under severe variation in exposure, including under- and overexposure. Rather than performing strict binary edge detection, the proposed approach focuses on enhancing and refining continuous-valued, gradient-based edge maps in illumination-degraded imagery where reliable ground truth annotations are typically unavailable.

The system is driven by a five-channel input tensor consisting of the histogram-adjusted luminance, multiscale Sobel gradients (3×3 and 5×5), a

global mean intensity map, and a histogram-derived scene flag. These cues are used to guide a modified U-Net architecture equipped with dynamic bright/dark branching, spatial attention, and a dual loss formulation in which luminance consistency is balanced with gradient preservation via a learnable weighting parameter. Following neural inference, an adaptive refinement module is applied to further improve the edge continuity and suppress illumination-dependent artifacts, through a process involving per-image parameter selection based on luminance statistics and multiscale gradient cues.

Within the NR evaluation framework applied here, the results indicate consistent edge enhancement behavior relative to classical Sobel baselines and stable performance trends compared with representative pre-trained learning-based edge detectors evaluated under the same conditions. The proposed hybrid formulation bridges the gap between deterministic gradient processing and illumination-aware feature learning, and supports interpretable and robust edge enhancement in scenarios with degraded illumination. The illumination-adaptive refinement behavior is driven by deterministic, statistics-based parameter selection, yielding stable and reproducible edge enhancement across the entire evaluation set.

8.2 Avenues for future research

In future work, the proposed system could be extended in several ways. The use of deeper or multiscale U-Net variants could be explored to strengthen contextual edge modeling under extreme exposure variation, which may improve contour continuity in heavily degraded regions. Richer multiscale fusion strategies for Sobel priors and refinement cues could further stabilize the balance between edge strengthening and noise suppression. The integration of complementary channel–spatial recalibration mechanisms (e.g., joint squeeze-and-excitation and spatial attention) may improve the sensitivity of the model to weak boundaries and reduce residual halo artifacts. Future research could also investigate spatially adaptive illumination estimation and region-aware feature routing to improve robustness under spatially varying illumination and mixed exposure conditions. Finally, broader statistical validation on larger and more diverse illumination-degraded datasets, including limited full-reference evaluation with manually annotated edge maps and a controlled human perceptual study, would enable a more comprehensive assessment of the robustness, perceptual edge continuity, and generalization of the model under real-world variability.

9 References

[1] R. C. Gonzalez, R. E. Woods: Digital Image Processing, 4th Edition, Pearson, New York, 2018.

[2] D. F. Chalob, B. A. Suhan, A. K. Hussein, R. H. Hasan: Edge Detection Methods: A Review, Journal of Computer Sciences and Informatics, Vol. 2, No. 4, May 2025, pp. 203 – 212.

[3] W. M. R. Wan Fadzli, A. Y. Dak, T. R. Razak: A Survey on Various Edge Detection Techniques in Image Processing and Applied Disease Detection, Journal of Computing Research and Innovation, Vol. 9, No. 2, September 2024, pp. 23 – 32.

[4] J. Canny: A Computational Approach to Edge Detection, IEEE Transactions on Pattern Analysis and Machine Intelligence, Vol. PAMI-8, No. 6, November 1986, pp. 679 – 698.

[5] R. Maini, H. Aggarwal: Study and Comparison of Various Image Edge Detection Techniques, International Journal of Image Processing, Vol. 3, No. 1, March 2009, pp. 1 – 11.

[6] M. A. Ansari, D. Kurchaniya, M. Dixit: A Comprehensive Analysis of Image Edge Detection Techniques, International Journal of Multimedia and Ubiquitous Engineering, Vol. 12, No. 11, November 2017, pp. 1 – 12.

[7] O. Ronneberger, P. Fischer, T. Brox: U-Net: Convolutional Networks for Biomedical Image Segmentation, Proceedings of the 18th International Conference Medical Image Computing and Computer-Assisted Intervention (MICCAI), Munich, Germany, October 2015, pp. 234 – 241.

[8] N. Siddique, S. Paheding, C. P. Elkin, V. Devabhaktuni: U-Net and Its Variants for Medical Image Segmentation: A Review of Theory and Applications, IEEE Access, Vol. 9, June 2021, pp. 82031 – 82057.

[9] S. Xie, Z. Tu: Holistically-Nested Edge Detection, International Journal of Computer Vision, Vol. 125, No. 1-3, December 2017, pp. 3 – 18.

[10] Y. Liu, M.- M. Cheng, X. Hu, J.- W. Bian, L. Zhang, X. Bai, J. Tang: Richer Convolutional Features for Edge Detection, IEEE Transactions on Pattern Analysis and Machine Intelligence, Vol. 41, No. 8, August 2019, pp. 1939 – 1946.

[11] Y. Li, L. Jin, M. Liu, Y. Mo, W. Zheng, D. Ge, Y. Bai: Research on Adaptive Edge Detection Method of Part Images Using Selective Processing, Processes, Vol. 12, No. 10, October 2024, p. 2271.

[12] S. S. Al Rawahi: A Comparison of Sobel and Prewitt Edge Detection Operators, East Journal of Computer Science, Vol. 1, No. 1, February 2025, pp. 49 – 58.

[13] M. H. Hesamian, S. Mashohor, M. I. Saripan, W. Wan Adnan: Scene Illumination Classification Using Illumination Histogram Analysis and Neural Network, Proceedings of the IEEE International Conference on Control System, Computing and Engineering, Penang, Malaysia, November 2013, pp. 290 – 295.

[14] M. M. Memon, M. A. Hashmani, A. Z. Junejo, S. S. Rizvi, A. A. Arain: A Novel Luminance-Based Algorithm for Classification of Semi-Dark Images, Applied Sciences, Vol. 11, No. 18, September 2021, p. 8694.

[15] S. W. Zamir, A. Arora, S. Khan, M. Hayat, F. S. Khan, M.- H. Yang, L. Shao: Multi-Stage Progressive Image Restoration, Proceedings of the IEEE/CVF Conference on Computer Vision and Pattern Recognition (CVPR), Nashville, USA, June 2021, pp. 14816 – 14826.

[16] J.- P. Hong, S.- J. Cho, J. Lee, S.- W. Ji, S.- J. Ko: Single Image Deblurring Based on Auxiliary Sobel Loss Function, Proceedings of the IEEE International Conference on Consumer Electronics - Asia (ICCE-Asia), Seoul, South Korea, November 2020, pp. 1 – 3.

[17] C. Guo, M. Szemenyei, Y. Yi, W. Wang, B. Chen, C. Fan: SA-UNet: Spatial Attention U-Net for Retinal Vessel Segmentation, Proceedings of the 25th International Conference on Pattern Recognition (ICPR), Milan, Italy, January 2021, pp. 1236 – 1242.

[18] Z. Al-Ameen, A. Muttar, G. Al-Badrani: Improving the Sharpness of Digital Image Using an Amended Unsharp Mask Filter, International Journal of Image, Graphics and Signal Processing (IJIGSP), Vol. 11, No. 3, March 2019, pp. 1 – 9.

[19] R. Zhao, Z. Wang, W. Guo, C. Zhang: Multi-Scene Image Enhancement Based on Multi-Channel Illumination Estimation, Expert Systems with Applications, Vol. 226, September 2023, p. 120271.

[20] F. Zhang, Y. Dai, X. Peng, C. Wu, X. Zhu, R. Zhou, Y. Wu: Brightness Segmentation-Based Plateau Histogram Equalization Algorithm for Displaying High Dynamic Range Infrared Images, Infrared Physics & Technology, Vol. 134, November 2023, p. 104894.

[21] A. Horé, D. Ziou: Image Quality Metrics: PSNR vs. SSIM, Proceedings of the 20th International Conference on Pattern Recognition, Istanbul, Turkey, August 2010, pp. 2366 – 2369.

[22] W. Piao, Y. Han, L. Hu, C. Wang: Quantitative Evaluation of Focus Measure Operators in Optical Microscopy, Sensors, Vol. 25, No. 10, May 2025, p. 3144.

[23] M. Zhu, L. Yu, Z. Wang, Z. Ke, C. Zhi: Review: A Survey on Objective Evaluation of Image Sharpness, Applied Sciences, Vol. 13, No. 4, February 2023, p. 2652.

[24] Y. Zhan, R. Zhang: No-Reference Image Sharpness Assessment Based on Maximum Gradient and Variability of Gradients, IEEE Transactions on Multimedia, Vol. 20, No. 7, July 2018, pp. 1796 – 1808.

[25] J. L. Pech-Pacheco, G. Cristobal, J. Chamorro-Martin, J. Fernandez-Valdivia: Diatom Autofocusing in Brightfield Microscopy: A Comparative Study, Proceedings of the 15th International Conference on Pattern Recognition (ICPR), Barcelona, Spain, September 2000, pp. 314 – 317.

[26] S. Yu, X. Zhang: Comprehensive Evaluation of Restoration Quality for Weak Image Signals with Fuzzy Logic, Systems Science & Control Engineering, Vol. 12, No. 1, December 2024, p. 2437257.

[27] M. A. Baig, A. A. Moinuddin, E. Khan, M. Ghanbari: DFT-Based No-Reference Quality Assessment of Blurred Images, Multimedia Tools and Applications, Vol. 81, No. 6, March 2022, pp. 7895 – 7916.

[28] X. Min, G. Zhai, K. Gu, X. Yang, X. Guan: Objective Quality Evaluation of Dehazed Images, IEEE Transactions on Intelligent Transportation Systems, Vol. 20, No. 8, August 2019, pp. 2879 – 2892.

[29] R. Sun, T. Lei, Q. Chen, Z. Wang, X. Du, W. Zhao, A. K. Nandi: Survey of Image Edge Detection, Frontiers in Signal Processing, Vol. 2, March 2022, p. 826967.

[30] S. Yang, T. Wu, S. Shi, S. Lao, Y. Gong, M. Cao, J. Wang, Y. Yang: MANIQA: Multi-Dimension Attention Network for No-Reference Image Quality Assessment, Proceedings of the IEEE/CVF Conference on Computer Vision and Pattern Recognition Workshops (CVPRW), New Orleans, USA, June 2022, pp. 1190 – 1199.

[31] Y. LeCun, Y. Bengio, G. Hinton: Deep Learning, Nature, Vol. 521, May 2015, pp. 436 – 444.

[32] F. Lu, C. Tang, T. Liu, Z. Zhang: SMA-Net: Sobel Operator Combined with Multi-Attention Networks for COVID-19 Lesion Segmentation, Proceedings of the 19th International Forum on Digital Multimedia Communications (IFTC), Shanghai, China, December 2022, pp. 377 – 390.

[33] F. Lu, C. Tang, T. Liu, Z. Zhang, L. Li: Multi-Attention Segmentation Networks Combined with the Sobel Operator for Medical Images, Sensors, Vol. 23, No. 5, February 2023, p. 2546.

[34] Z. Yin, Z. Wang, C. Fan, X. Wang, T. Qiu: Edge Detection via Fusion Difference Convolution, Sensors, Vol. 23, No. 15, August 2023, p. 6883.

[35] X. Guo, Y. Li, H. Ling: LIME: Low-Light Image Enhancement via Illumination Map Estimation, IEEE Transactions on Image Processing, Vol. 26, No. 2, February 2017, pp. 982 – 993.

[36] J. Jing, S. Liu, G. Wang, W. Zhang, C. Sun: Recent Advances on Image Edge Detection: A Comprehensive Review, Neurocomputing, Vol. 503, September 2022, pp. 259 – 271.

[37] H. Spontón, J. Cardelino: A Review of Classic Edge Detectors, Image Processing on Line, Vol. 5, June 2015, pp. 90 – 123.

[38] M. J. Meester, A. S. Başlamişli: SAR Image Edge Detection: Review and Benchmark Experiments, International Journal of Remote Sensing, Vol. 43, No. 14, October 2022, pp. 5372 – 5438.

[39] G. Madhavi, R. D. Sathiya: An Extensive Study on Edge Detection Methods: A Review, AIP Conference Proceedings, Vol. 3028, No. 1, July 2024, p. 020042.

[40] G. Hu: A Mathematical Survey of Image Deep Edge Detection Algorithms: From Convolution to Attention, Mathematics, Vol. 13, No. 15, July 2025, p. 2464.

[41] Z. Su, J. Zhang, L. Wang, H. Zhang, Z. Liu, M. Pietikäinen, L. Liu: Lightweight Pixel Difference Networks for Efficient Visual Representation Learning, IEEE Transactions on Pattern Analysis and Machine Intelligence, Vol. 45, No. 12, December 2023, pp. 14956 – 14974.

[42] X. Soria, Y. Li, M. Rouhani, A. D. Sappa: Tiny and Efficient Model for the Edge Detection Generalization, Proceedings of the IEEE/CVF International Conference on Computer Vision Workshops (ICCVW), Paris, France, October 2023, pp. 1356 – 1365.

[43] X. Soria, A. Sappa, P. Humanante, A. Akbarinia: Dense Extreme Inception Network for Edge Detection, Pattern Recognition, Vol. 139, July 2023, p. 109461.

[44] X. Qin, Z. Zhang, C. Huang, C. Gao, M. Dehghan, M. Jagersand: BASNet: Boundary-Aware Salient Object Detection, Proceedings of the IEEE/CVF Conference on Computer Vision and Pattern Recognition (CVPR), Long Beach, USA, June 2019, pp. 7471 – 7481.

[45] J. He, S. Zhang, M. Yang, Y. Shan, T. Huang: Bi-Directional Cascade Network for Perceptual Edge Detection, IEEE Transactions on Pattern Analysis and Machine Intelligence, Vol. 44, No. 1, January 2022, pp. 100 – 113.

[46] Z. Yu, C. Feng, M.- Y. Liu, S. Ramalingam: CASENet: Deep Category-Aware Semantic Edge Detection, Proceedings of the IEEE Conference on Computer Vision and Pattern Recognition (CVPR), Honolulu, USA, July 2017, pp. 1761 – -1770.

[47] Z. Yu, W. Liu, Y. Zou, C. Feng, S. Ramalingam, B. V. K. Vijaya Kumar, J. Kautz: Simultaneous Edge Alignment and Learning, Proceedings of the 15th European Conference on Computer Vision (ECCV), Munich, Germany, September 2018, pp. 400 – 417.

[48] Y. Liu, M.- M. Cheng, D.- P. Fan, L. Zhang, J.- W. Bian, D. Tao: Semantic Edge Detection with Diverse Deep Supervision, International Journal of Computer Vision, Vol. 130, No. 1, January 2022, pp. 179 – 198.

[49] X. Luo, Z. Ai, Q. Liang, Y. Xie, Z. Shi, J. Fan, Y. Qu: EdgeFormer: Edge-Aware Efficient Transformer for Image Super-Resolution, IEEE Transactions on Instrumentation and Measurement, Vol. 73, August 2024, p. 5029312.

[50] A. S. Abosinnee, G. Bencsik, F. Abedi: Edges in Image with Illumination Variations Scenarios: A Review, The Visual Computer, Vol. 41, No. 14, November 2025, pp. 12277 – 12305.

[51] R. Ranjan, A. Prasad: Optimizing Image Edge Detection: Fusing Sobel and Robert via Convolutional Neural Networks for Enhanced Performance, Proceedings of the International Conference on Artificial Intelligence and Emerging Technology (Global AI Summit), Greater Noida, India, September 2024, pp. 705 – 710.

[52] R. Ranjan, A. Prasad: A Novel Hybrid Deep Learning Model for Image Edge Detection, Proceedings of the International Conference on Augmented Reality, Intelligent Systems, and Industrial Automation (ARIIA), Manipal, India, December 2024, pp. 1 – 7.

[53] A. Verma, N. Dhanda, V. Yadav: Enhancing Image Segmentation through an Innovative Hybrid Kernel: A Weighted Fusion of Sobel and Prewitt Operators Using Artificial Neural Networks, Proceedings of the International Conference on Computing, Sciences and Communications (ICCSC), Ghaziabad, India, October 2024, pp. 1 – 5.

[54] I. Sobel, G. Feldman: A 3×3 Isotropic Gradient Operator for Image Processing, Stanford Artificial Intelligence Project (SAIL), 1968, pp. 271 – 272, Subsequently described in R. O. Duda, P. E. Hart: Pattern Classification and Scene Analysis, John Wiley & Sons, New York, 1973.

[55] Studio Encoding Parameters of Digital Television for Standard 4:3 and Wide-Screen 16:9 Aspect Ratios, Recommendation ITU-R BT.601-7, March 2011. Available at: https://www.itu.int/dms_pubrec/itu-r/rec/bt/R-REC-BT.601-7-201103-I!!PDF-E.pdf

[56] MathWorks: Convert RGB Image or Colormap to Grayscale, MATLAB Documentation, 2023, Available at: https://nl.mathworks.com/help/matlab/ref/rgb2gray.html

[57] H. Lu, Y. She, J. Tie, S. Xu: Half-UNet: A Simplified U-Net Architecture for Medical Image Segmentation, Frontiers in Neuroinformatics, Vol. 16, June 2022, p. 911679.

[58] B. Pang, L. Chen, Q. Tao, E. Wang, Y. Yu: GA-UNet: A Lightweight Ghost and Attention U-Net for Medical Image Segmentation, Journal of Imaging Informatics in Medicine, Vol. 37, No. 4, August 2024, pp. 1874 – 1888.

[59] C. Shorten, T. M. Khoshgoftaar: A Survey on Image Data Augmentation for Deep Learning, Journal of Big Data, Vol. 6, No. 1, December 2019, p. 60.

[60] Z. Fu, Y. Zheng, T. Ma, H. Ye, J. Yang, L. He: Edge-Aware Deep Image Deblurring, Neurocomputing, Vol. 502, September 2022, pp. 37 – 47.

[61] C. Guo, C. Li, J. Guo, C. C. Loy, J. Hou, S. Kwong, R. Cong: Zero-Reference Deep Curve Estimation for Low-Light Image Enhancement, Proceedings of the IEEE/CVF Conference on Computer Vision and Pattern Recognition (CVPR), Seattle, USA, June 2020, pp. 1777-1786.

[62] C. Li, C. Guo, C. C. Loy: Learning to Enhance Low-Light Image via Zero-Reference Deep Curve Estimation, IEEE Transactions on Pattern Analysis and Machine Intelligence, Vol. 44, No. 8, August 2022, pp. 4225 – 4238.

[63] C. Zhao, W. Yue, J. Xu, H. Chen: Joint Low-Light Image Enhancement and Denoising via a New Retinex-Based Decomposition Model, Mathematics, Vol. 11, No. 18, September 2023, p. 3834.

[64] R. L. Wasserstein, N. A. Lazar: The ASA Statement on p-Values: Context, Process, and Purpose, The American Statistician, Vol. 70, No. 2, June 2016, pp. 129 – 133.

[65] N. M. White, T. Balasubramaniam, R. Nayak, A. G. Barnett: An Observational Analysis of the Trope "A p-Value of < 0.05 was Considered Statistically Significant" and Other Cut-and-Paste Statistical Methods, PLoS One, Vol. 17, No. 3, March 2022, p. e0264360.

[66] H. He, B. Jiang, C. Shi, Y. Lu, Y. Lin: An Objective Evaluation Method for Image Sharpness Under Different Illumination Imaging Conditions, Photonics, Vol. 11, No. 11, November 2024, p. 1032.

[67] H. Khan, M. T. Rasheed, S. Zhang: Illuminating the Darkness: Experimental Review of Cutting-Edge Deep Learning Techniques for Low-Light Image Enhancement, Cluster Computing, Vol. 28, No. 11, October 2025, p. 729.

[68] M. T. Rasheed, H. Khan, J. Wang, Y. Kang: Advancing Low-Light Image Enhancement Through Deep Learning: A Comprehensive Experimental Study, Knowledge-Based Systems, Vol. 325, September 2025, p. 113827.